

Impact of transition metal ion Co^{2+} on structural and optical properties of ZnO nanoparticles synthesised by co-precipitation method

P.Geetha Devi¹, A.Sakthi Velu²

1. Assistant Professor, Department of Physics, M.A.M College of Engineering, Siruganur, Tiruchirappalli – 621105.

2. Assistant Professor, PG & Research Department of Physics, Periyar E.V.R. College (Autonomous), Tiruchirappalli -620023.

Abstract

Pure Zinc oxide (ZnO NPs), $\text{Zn}_{0.70}\text{Co}_{0.30}\text{O}$ and $\text{Zn}_{0.50}\text{Co}_{0.50}\text{O}$ nanoparticles (NPs) were synthesized by the co-precipitation method. The synthesized nanoparticles retained the wurtzite hexagonal structure, which was confirmed by the X-ray diffraction studies. The oxidation states of the elements O (1s), Zn (2p), and Co (2p) were confirmed by XPS studies. HRTEM images showed that the particles sizes were approximately 20-40 nm and spherical shape for pure and hexagonal shape both $\text{Zn}_{0.70}\text{Co}_{0.30}\text{O}$ and $\text{Zn}_{0.50}\text{Co}_{0.50}\text{O}$ NPs respectively. The FT-IR spectra confirmed the Zn-O stretching bands range at 421 to 495 cm^{-1} for ZnO NPs. From the UV-VIS spectroscopic measurements, the excitonic peaks were found around 393, 399 and 396 nm for the respective samples. The photoluminescence measurements revealed that the broad emission composed of five different bands due to zinc and oxygen vacancies.

Key Word: ZnO NPs, XRD, XPS and HRTEM

Introduction

The size and shape-controlled Zinc oxide nanostructures are very important in controlling their physical and chemical properties for their prospective applications. The optical properties of nanocrystalline semiconductors have been studied widely in recent years. As the size of the material becomes smaller and the band gap becomes larger, this changes the optical, electrical and magnetic properties of the substance, making it suitable for new applications and devices. Among them, the impurity atoms doping with semiconductor substance can be changed in their electrical, magnetic and optical properties [1-6].

Significant interest has been also focused on diluted magnetic semiconductors (DMS) because of their rare optical properties and potential application in optoelectronic devices [7, 8]. The DMS's are characterized by the limited change of cations of the nonmagnetic semiconductors by magnetic

Transition-metal ions. Among these semiconductors, ZnO doped with a small amount of transition metal ions, in particular with cobalt ions, has been vastly observed, because it offers an effective method to adjust its electrical [9], optical and magnetic properties, with no crystal structural change [10-12]. Among these, Co is reported as an important metal for incorporation into the ZnO lattice due to its abundant electron states and large solubility in its matrix [13, 14].

Numerous approaches are available for the synthesis of ZnO nanoparticles, such as a Green method [15, 16] and chemical or physical technique, [17] hydrothermal process [18], sol-gel technique, [19] and co-precipitation technique [20]. Among the various techniques, co-precipitation is one of the most important techniques to prepare the nanoparticles. The co-precipitation technique reduces the temperature of the reaction where a homogeneous mixture of reagent precipitates. It is an

easy technique for the synthesis of metal oxides nanoparticles, which are highly reactive in low temperature sintering.

In order to explore new schemes to identify and develop the next generation of optical, electrical and magnetic materials are very important in the fast growth world. In present investigation, pure ZnO, $Zn_{0.70}Co_{0.30}O$ and $Zn_{0.50}Co_{0.50}O$ NPs were prepared by co-precipitation technique. The pure and doped ZnO NPs are studied with the support of the structural and optical characterization studies.

Experimental Section

The prepared pure, $Zn_{0.70}Co_{0.30}O$ and $Zn_{0.50}Co_{0.50}O$ NPs were using analytical grade Zinc (II) nitrate hexahydrate ($Zn(NO_3)_2 \cdot 6H_2O$), Cobalt nitrate hexahydrate ($Co(NO_3)_2 \cdot 6H_2O$), Poly Ethylene Glycol (PEG) and sodium hydroxide (NaOH) in as-received condition without further purification.

In synthesis of ZnO NPs, 0.1 M of Zinc (II) nitrate hexahydrate and 0.8 M of NaOH and 5.0 g of PEG were separately dissolved in each 100 ml of distilled water using three 200 ml beakers. At first, Zinc Nitrate and PEG solutions were mixed homogeneously. Next, NaOH solution was added drop wise to the homogenous mixed solution, yielding a white precipitate. The solution with the white precipitate was stirred at the room temperature for 30 min, and then at temperature of 60 °C for 4 hours. This solution was refluxed at room temperature for 24 hours. Then, a clear solution was obtained, which found to be stable at ambient condition. Thereafter, the solution was washed several times with double distilled water and ethanol. Finally, the precipitate was dried at 120 °C.

For the synthesis of $Zn_{0.70}Co_{0.30}O$ and $Zn_{0.50}Co_{0.50}O$ NPs, the calculated amount of (0.30 M and 0.50 M) of aqueous Cobalt nitrate hexahydrate solutions were added into (0.70 M and 0.50 M) of aqueous Zinc Nitrate solution. This solution was mixed into 100 ml of an aqueous solution containing 5.0 g of PEG.

0.8M of aqueous NaOH solution was added drop wise to this homogenous mixture to form a brown precipitate. The solution with the brown precipitate was processed as above to obtain Zn_{0.70}Co_{0.30}O and Zn_{0.50}Co_{0.50}O samples. The solution with the brown precipitate were stirred at the room temperature for 30 min, and then at temperature of 60 °C for 4 hours. These solutions were refluxed at room temperature for 24 hours. Then, a clear solutions were obtained, which found to be stable at ambient condition. Thereafter, the solutions were washed several times with double distilled water and ethanol. Finally, the precipitate were dried at 120 °C Thus, pure, Zn_{0.70}Co_{0.30}O and Zn_{0.50}Co_{0.50}O samples were obtained. These samples were annealed at 600°C for 4 hours because the energy from the heat could enhance the vibration and diffusion of lattice atoms for atomic for crystallization.

Characterization techniques

The structural analysis of the synthesized pure, Zn_{0.70}Co_{0.30}O and Zn_{0.50}Co_{0.50}O samples are carried out using a powder X-ray diffractometer (PANalytical X'Pert Pro) with a Cu-K α radiation source (wavelength: 1.5418 Å). XPS measurements were performed with an XPS instrument (Carl Zeiss) equipped with an Ultra 55 FESEM with EDS, and all the spectra were recorded under ultrahigh vacuum with Al K α excitation at 250 W. The morphology of the synthesized ZnO samples were examined using TEM. Samples for TEM analysis were prepared by drop coating the nanoparticle solutions on carbon-coated copper grids at room temperature. The excess nanoparticle solution was removed with filter paper. The copper grid was finally dried at room temperature and was subjected to TEM analysis by the instrument Tecnai F20model operated at an accelerating voltage of 200 kV. For the spectroscopic study, the FTIR spectra were recorded in the range of 400–4000 cm⁻¹ using a Perkin–Elmer

spectrometer. The absorption spectra of samples were studied in the range between 200 and 800 nm by JASCO V-650 spectro-photometer. Photoluminescence spectra were taken using spectrometer Cary Eclipse EL0808351.

Results and Discussion

XRD analysis

Figure.1 shows the XRD patterns of pure, Zn_{0.70}Co_{0.30}O and Zn_{0.50}Co_{0.50}O NPs nanocrystalline powders for different Co concentrations, sintered in air at 700 °C for 5 h. The patterns were indexed all peaks were well matched with hexagonal structure of ZnO using the standard data (JCPDS-36-1451) [21], without any other impure phases regardless of dopant concentrations. Thus, the wurtzite structure not modified by the addition of Co ion into the ZnO matrix indicates that the Co dopant ought to be incorporated into the lattice as sub-situational ion [22]. In order to study the effect of Co doping, a careful analysis of the XRD peaks indicate that there is a significant shifting and broadening in (0 0 2) peak position toward higher 2 θ value with increasing of Co content as shown in the inset of Fig. 2. No considerable changes in the lattice parameters are found for different Co doping concentrations but to be reported it is decreasing up to 30% of Co concentration and further increases for 50%. Since the ionic radius of Co²⁺ is close to that of Zn²⁺, the change in full width at half maxima (FWHM) is due to particle size variation given in the Table (1(a-b)). Changes in the FWHM are in accordance with the particle size which was calculated from the Debye–Scherrer's formula

$$D = \frac{k\lambda}{\beta_D \cos\theta} \quad (1)$$

where λ is the X-ray wavelength (Cu K α = 1.5418 Å), β is the full width at half maximum of the most intense peak and θ is the peak position [23].

Using above equation we evaluated crystallite size for different samples and listed in Table 2.

It is evident that the FWHM gradually increases with the increase in doping content up to 30% while it lowers for the 50% Co concentration, which intern increases the crystallite size up to the same content of Co. It depends on the reason that the growth of ZnO grains is determined by the movement and the diffusion of Zn^{2+} . However, in the Co doped ZnO, Co may exist as the grain boundary which can enhance the energy barrier of the movement and the diffusion of Zn^{2+} and increases the electrical resistivity, therefore restrain the growth of ZnO grains [24,25]. Doped Co is acting as an electrical dopant at initial doping concentration but as an impurity at higher doping concentration. Existence of impurities increases the electrical conductivity because it can diffuse [26]. Thus, favours the phenomenon of grain growth in case of 50% Co doped ZnO.

The lattice parameters of semiconductors usually depend on the foreign atoms, defects and the difference in ionic radii with respect to the substituted matrix ions. The difference in the ionic radii of Co^{2+} with respect to Zn^{2+} gives the variation of the lattice constants. The lattice parameters for hexagonal ZnO NPs were estimated from the equation [27],

$$\frac{1}{d_{hkl}^2} = \frac{4}{3(h^2 + hk + k^2/a^2)} + \frac{l^2}{c^2} \quad (2)$$

where a and c are the lattice parameters; h, k and l are the Miller indices; d_{hkl} is the interplaner spacing for the plane (h k l). For pure ZnO NPs, the values of the lattice parameters 'a' and 'c' are estimated to be 3.25Å and 5.21 Å, respectively. The substitution of Co^{2+} ions in the place of Zn^{2+} ions increases the

values (see Table-2) of the lattice constants 'a' and 'c' for the doped ZnO NPs, due to the substitution of Co^{2+} ions in the ZnO lattice.

X-ray photoelectron spectroscopy

X-ray photoelectron spectroscopy study is one of the important tools to identify the surface valence state of the elements in a material. In the present investigation, the composition and structure of the prepared $Zn_{0.50}Co_{0.50}O$ NPs samples are shown in Fig. 3 and wide scan result is shown in Fig. 2(a). According to Fig. 2(b), due to strong spin orbit coupling Zn (2p) signal splits into two symmetrical peaks as Zn 2p_{3/2} and Zn 2p_{1/2}. These peaks centered at 1021.30 eV and 1044.47 eV respectively, with a spin-orbit splitting value of 23.17 eV, which coincides with the findings for Zn^{2+} bound to oxygen in the ZnO matrix [28].

The Co (2p) signals are divided into three symmetrical signals, namely G1, G2 and G3 in the Gaussian fitting (see Fig. 2c). Among these, the lower energy level (G1) of the Co (2p) signal at 780.56 eV is assigned to the Co 2p_{3/2} electrons and middle energy level (G2) of the Co (2p) signal at 795.68 eV is associated with Co 2p_{1/2} electrons. The binding energy difference of Co 2p ionic state is 15.12 eV [2]. It has been reported that the value of the difference in binding energies is 15.2 eV for Co 2p ions [29].

The asymmetric O (1s) signals are divided into three symmetrical signals (see Fig. 2d), namely U1, U2 and U3 in the Gaussian fitting, peak U1 centered at 529.80 eV is attributed to the ZnO Crystal lattice oxygen. The peaks U2 at 531.20 eV and U3 at 531.55 eV are associated with oxygen-deficient regions in the ZnO matrix, as well as the chemisorbed oxygen of the surface hydroxyl, $-CO_3$, absorbed H_2O or absorbed O_3 [30].

TEM analysis

Figure 3 (a-c) shows high resolution transmission electron microscope images of the as-prepared pure, $Zn_{0.70}Co_{0.30}O$ and $Zn_{0.50}Co_{0.50}O$ NPs calcined at temperature $700^{\circ}C$, and insets shows the electron diffraction FT-IR spectroscopic analysis reveals the vibrational frequencies of the pure, $Zn_{0.70}Co_{0.30}O$ and $Zn_{0.50}Co_{0.50}O$ samples. The recorded FT-IR spectra are shown in Fig. 4. Table 3 represents the FT-IR Peak Assignments. The peak in the range of $3020-3650\text{ cm}^{-1}$ corresponds to the vibrational mode of O-H bonds [31]. The absorption peaks are observed at 3398 , 3397 and 3393 cm^{-1} for pure, $Zn_{0.70}Co_{0.30}O$ and $Zn_{0.50}Co_{0.50}O$ samples respectively due to the O-H stretching of surface-absorbed water molecules [32]. The peak at 2950 cm^{-1} is due to asymmetric C-H bond. At 2923 cm^{-1} the weak intensity of the asymmetric stretching mode of the CH_2 group in PEG can also observed for pure and $Zn_{0.70}Co_{0.30}O$ NPs. The asymmetric stretching vibration of C-O is observed at 1518 cm^{-1} for the $Zn_{0.70}Co_{0.30}O$ and $Zn_{0.50}Co_{0.50}O$ samples. The symmetric C=O bands are observed at 1415 cm^{-1} for Co doped ZnO samples. The medium to weak band at 872 cm^{-1} is assigned to the metal-oxygen vibration frequency due to the changes in the microstructural features by the addition of Co into the Zn-O lattice [29]. In present investigation, metal and oxygen (Zn-O) vibration bands observed at 884 and 838 cm^{-1} for pure, $Zn_{0.70}Co_{0.30}O$ and $Zn_{0.50}Co_{0.50}O$ NPs respectively. The symmetric C=O bands are observed at 1415 cm^{-1} for Co doped ZnO samples. The bands are observed at 699 and 675 cm^{-1} due to the Zn-O bending vibration for pure and Co doped ZnO NPs respectively. In

patterns. The particles sizes are approximately $20-40\text{ nm}$ and spherical shape for pure ZnO NPs and hexagonal shape both $Zn_{0.70}Co_{0.30}O$ and $Zn_{0.50}Co_{0.50}O$ NPs respectively.

FT-IR analysis

literature, the absorption peaks at 560 cm^{-1} and 402 cm^{-1} assigned to the stretching vibration of Zn-O bonds from ZnO nanoparticles [33]. In our results Zn-O bands are observed at 533 to 597 cm^{-1} and 421 to 495 cm^{-1} for pure and Co doped ZnO nanoparticles. In FTIR spectra, Zn-O stretching bands were observed at 533 to 597 cm^{-1} and 421 to 495 cm^{-1} for pure and Co doped ZnO NPs.

FT-IR analysis

The optical absorption measurements of the pure, $Zn_{0.70}Co_{0.30}O$ and $Zn_{0.50}Co_{0.50}O$ samples were carried out by UV-Vis spectroscopy. The absorbance is expected to depend on various aspects, such as band gap, oxygen deficiency surface roughness and impurity centers [34]. Absorbance spectra shows an absorption edge at around 393 , 399 and 396 nm for pure and Co doped ZnO NPs (see Fig. 5), which can be attributed to the photo-excitation of electrons from valence band to conduction band. The absorption edge of different samples slightly varies as the concentration of Co in the ZnO nanoparticles fluctuates. The position of the absorption spectra is observed to shift toward the higher wavelength sided with increase in Co doping concentration in ZnO.

The band-gap energy (E_g) values for the samples were evaluated by plot between $(\alpha h\nu)^2$ versus photon energy ($h\nu$) are calculated using classical Tauc relation [35] Figure 5 (a-c) shows that the band gap energy is decreases from 3.15

eV to 3.1 eV for pure and Co doped ZnO NPs. The reduction of the bandgap in heavily doped semiconductor can be consistent out by many reasons. The main contributions are increase in crystalline size, impurity band formation, band-band transition due to several defect, bandgap bowing effect etc., [36]. In our result, the bandgap reduction observed in Co doped ZnO is purely exposed to difference in crystallite size due to Co incorporation. Thus, a red shift phenomenon is revealed, where the Co doping results in decrease in optical bandgap deviating. The Photoluminescence emission spectra of pure, Co doped ZnO samples using excitation wavelength at 325 nm and covering from the very short wavelength of 370 nm to long wavelength 550 nm as shown in Fig.6 (a-c). A good fit of five peaks Gaussian function is obtained for all the PL spectra of the samples at the bottom labelled as S1, S2, S3, S4 and S5.

Pure, Co doped ZnO NPs emission values are given in the Table 4. The observation of visible emissions is related to intrinsic defects in ZnO, which include Zn vacancies (V_{Zn}), O vacancies (V_O), interstitial Zn (Zn_i), interstitial O (O_i), and substitution of O at Zn position (O_{Zn}) [40-42]. The near-band emission (NBE) peak S1 is observed at 391 nm for ZnO NPs [43-45] and this corresponds to the radiative recombination of the free exciton-exciton collision process in the ZnO NPs. The violet emission peak (S2) probably due to the radiative defects of Zn_i and V_{Zn} related to the interface traps existing at the grain boundaries of ZnO and this peak observed at 411 nm [46]. The peak S3 at 444 nm is correspond to the blue emission [47], caused by two defect's level, either transition from Zn_i to the valence band or transition from the bottom of the conduction band to the O_i level. The blue-green emission peak S4 is centered at 490 nm,

from the Burstein-Moss shift [37-39]. The estimated bandgap values are near to that of bulk ZnO. This gives a conclusion that there is no symptom of quantum size confinement. The bandgap of Co doped ZnO NPs shows a non-monotonic dependence on the Co concentration, as shown in Fig. 5(a-c). Among this, the bandgap of ZnO NPs as a role of the Co content strongly supports that Co is indeed localized into the host lattice of ZnO.

Photoluminescence emission spectra analysis

due to a surface defects in the ZnO NPs corresponding to the transition between V_o and O_i defect [48]. Finally the peak S5 that arose at 520 nm represents green emission [49, 50], this is due to the impurity levels corresponding to the singly ionized V_o in the ZnO NPs.

The values of the S1, S2, S3, S4 and S5 emission bands of $Zn_{0.70}Co_{0.30}O$ and $Zn_{0.50}Co_{0.50}O$ are shown in Fig. b-c (see Table 4), using the excitation wavelength of 325 nm. Among these, the NBE emission of pure ZnO (391 nm) is shift towards lower wavelength side for $Zn_{0.70}Co_{0.30}O$ (380 nm) and $Zn_{0.50}Co_{0.50}O$ (372 nm) NPs respectively. These shifts are occurring due to the dopant Co^{2+} ions substituted in Zn^{2+} ions. But the Co-doped ZnO NPs, the blue emissions values (444-436 nm) of the decrease due to the distortion in the host ZnO lattice by the Co metal ion impurities. However, the Co-doped ZnO NPs increase the violet emissions from 411 to 415 nm and respectively, which may also induce some broadening but not play a major role. The $Zn_{0.70}Co_{0.30}O$ and $Zn_{0.50}Co_{0.50}O$ NPs increase the Blue-green band emission (S4) and Green band emissions (S5) as compared to the pure ZnO NPs. intensity of the green emission peaks is increased with respect to the increasing doping level of Co^{2+} . It has been reported that the green

emission peaks are due to the oxygen vacancies and transition of a photogenerated electron from the conduction band to a deeply trapped hole

Conclusions

In summary, pure, $Zn_{0.70}Co_{0.30}O$ and $Zn_{0.50}Co_{0.50}O$ were prepared through the co-precipitation method. The X-ray diffraction studies were confirmed that the prepared particles were of the hexagonal wurtzite structure. The substitution of Co^{2+} ions in the place of Zn^{2+} ions increased the lattice constants values 'a' and 'c' for the doped ZnO NPs, due to the substitution effect of Co^{2+} ions in the ZnO lattice. The XPS studies showed that from the indexed peaks corresponding to C (1s), Zn (2p), Co (2p) and O (1s), respective binding energies of the elements were estimated. From the HRTEM images, the particles size were approximately 20-40 nm for spherical shaped for pure ZnO NPs and hexagonal shaped both $Zn_{0.70}Co_{0.30}O$ and $Zn_{0.50}Co_{0.50}O$ NPs. The band gap of ZnO and Co doped ZnO NPs were estimated as 3.15, 3.1 and 3.125 eV from the UV-Vis spectroscopic measurements. The photoluminescence studies showed that the doping of ZnO altered the band emission, which is due to zinc vacancies, oxygen vacancies and surface defects. The ZnO NPs received much attention for their potential application in cancer therapy. The ZnO NPs are used in cancer therapy and their inherent preferential cytotoxicity against cancer cells can be used for new anti-cancer agents. The anticancer efficiency of ZnO NPs generally depends on the presence of more ROS, which was mainly attributed to the increase in oxygen vacancies. The ZnO NPs as compare to the Co-doped ZnO NPs oxygen vacancies were increased.

[51]. These changes in the emissions confirm the substitution of the metal ion Co^{2+} into the ZnO lattice.

References

- [1] Hsu, L., Yeh, C. S., Kuo, C. C., Huang, B. R., & Dhar, S. Optical and transport properties of undoped and Al-, Ga-and In-doped ZnO thin films. *Journal of Optoelectronics and Advanced Materials*, 7 (2005) 3039.
- [2] Bhargava, R. N., Haranath, D., & Mehta, A. Bandgap engineering and doping of ZnO and ZnOS nanocrystals. *Journal of Korean Physical Society*, 53 (2008) 2847.
- [3] Bae, S. Y., Na, C. W., Kang, J. H., & Park, J. Comparative structure and optical properties of Ga-, In-, and Sn-doped ZnO nanowires synthesized via thermal evaporation. *The Journal of Physical Chemistry B*, 109 (2005) 2526-2531.
- [4] Radovanovic, P. V., & Gamelin, D. R. High-Temperature Ferromagnetism in Ni²⁺-Doped ZnO Aggregates Prepared from Colloidal Diluted Magnetic Semiconductor Quantum Dots. *Physical review letters*, 91 (2003) 157202.
- [5] Norberg, N. S., Kittilstved, K. R., Amonette, J. E., Kukkadapu, R. K., Schwartz, D. A., & Gamelin, D. R. Synthesis of colloidal Mn²⁺: ZnO quantum dots and high-TC ferromagnetic nanocrystalline thin films. *Journal of the American Chemical Society*, 126 (2004) 9387-9398.
- [6] Ueda, K., Tabata, H., & Kawai, T. Magnetic and electric properties of transition-metal-doped ZnO films. *Applied Physics Letters*, 7 (2001)988-990.

- [7] Varshney, P., Srinet, G., Kumar, R., Sajal, V., Sharma, S. K., Knobel, M., ... & Kulriya, P. K. Room temperature ferromagnetism in sol-gel prepared Co-doped ZnO. *Materials Science in Semiconductor Processing*, 15 (2012) 314-318.
- [8] Caglar, Y. Sol-gel derived nanostructure undoped and cobalt doped ZnO: Structural, optical and electrical studies. *Journal of alloys and Compounds*, 560 (2013) 181-188.
- [9]. Ko, T. Y., Tsai, M. H., Lee, C. S., & Sun, K. W. Electron transport mechanisms in individual cobalt-doped ZnO nanorods. *Journal of Nanoparticle Research*, 14 (2012) 1-12.
- [10]. Li, P., Wang, S., Li, J., & Wei, Y. Structural and optical properties of Co-doped ZnO nanocrystallites prepared by a one-step solution route. *Journal of Luminescence*, 132 (2012) 220-225.
- [11] Wang, S., Li, P., Liu, H., Li, J., & Wei, Y. The structure and optical properties of ZnO nanocrystals dependence on Co-doping levels. *Journal of Alloys and Compounds*, 505 (2010) 362-366.
- [12] Li, B., Chen, Z., Boafu, F., Shen, H., & Luo, J. Dopant position of Co atom in Zn_{1-x}Co_xO nanoparticles studied by extended X-ray absorption fine structure. *Journal of sol-gel science and technology*, 66 (2013) 163-167.
- [13] De Carvalho, H. B., De Godoy, M. P. F., Paes, R. W. D., Mir, M., De Zevallos, A. O., Iikawa, F., ... & Sabioni, A. C. S. Absence of ferromagnetic order in high quality bulk Co-doped ZnO samples. *Journal of applied physics*, 108 (2010) 033914.
- [14] Hao, H., Qin, M., & Li, P. Structural, optical, and magnetic properties of Co-doped ZnO nanorods fabricated by a facile solution route. *Journal of Alloys and Compounds*, 515 (2012) 143-148.
- [15] Ali, M. R., Umaralikhan, L., & Jaffar, M. (2015). Antibacterial Effect of Silver Nanoparticles Synthesized Using Curcuma Aromatica Leaf Extract.
- [16] Umaralikhan, L., & Jaffar, M. J. M. Green Synthesis of MgO Nanoparticles and its Antibacterial Activity. *Iranian Journal of Science and Technology, Transactions A: Science*, 1-9.
- [17] Djerdj, I., Garnweitner, G., Arčon, D., Pregelj, M., Jagličić, Z., & Niederberger, M. Diluted magnetic semiconductors: Mn/Co-doped ZnO nanorods as case study. *Journal of Materials Chemistry*, 18 (2008) 5208-5217.
- [18] Zhang, L., Liu, X., Geng, C., Fang, H., Lian, Z., Wang, X., ... & Yan, Q. Hexagonal crown-capped zinc oxide micro rods: hydrothermal growth and formation mechanism. *Inorganic chemistry*, 52 (2013) 10167-10175.
- [19] Chakraborti, S., Sarwar, S., & Chakrabarti, P. The effect of the binding of ZnO nanoparticle on the structure and stability of α -lactalbumin: a comparative study. *The Journal of Physical Chemistry B*, 117 (2013) 13397-13408.
- [20] Zhang, S., Hu, F., He, J., Cheng, W., Liu, Q., Jiang, Y., ... & Wei, S. Interplay between Occupation Sites of (Co, Cu) Codopants and Crystal Orientation of ZnO Matrix. *The Journal of Physical Chemistry C*, 117 (2013) 24913-24919.
- [21] File, P. D. Joint committee on powder diffraction standards. ASTM, Philadelphia, (1967) 9-185.

- [22] Vijayaprasath, G., Murugan, R., & Ravi, G. Structural, optical and magnetic properties of Ni doped ZnO nanostructures prepared by coprecipitation method. *J. Chem. Tech. Res*, 6 (2014) 3385-3387.
- [23] Cullity Deceased, B. D., & Stock, S. R. *Elements of X-ray Diffraction*. (2001).
- [24] Yan, Q., Chen, J. Z., & Tu, M. J. Effects of additive Nd₂O₃ on varistor voltage and microstructure of ZnO varistor. *Journal of Rare Earths*, 21 (2003) 142.
- [25] Vijayaprasath, G., Murugan, R., Mahalingam, T., Hayakawa, Y., & Ravi, G. Enhancement of ferromagnetic property in rare earth neodymium doped ZnO nanoparticles. *Ceramics International*, 41 (2015) 10607-10615.
- [26] Ansari, S. A., Nisar, A., Fatma, B., Khan, W., & Naqvi, A. H. Investigation on structural, optical and dielectric properties of Co doped ZnO nanoparticles synthesized by gel-combustion route. *Materials Science and Engineering: B*, 177 (2012) 428-435.
- [27] Vijayaprasath, G., Murugan, R., Palanisamy, S., Prabhu, N. M., Mahalingam, T., Hayakawa, Y., & Ravi, G. Structural, optical and antibacterial activity studies of neodymium doped ZnO nanoparticles. *Journal of Materials Science: Materials in Electronics*, 26 (2015) 7564-7576.
- [28] Chastain, J., & King, R. C. (Eds.). *Handbook of X-ray photoelectron spectroscopy: a reference book of standard spectra for identification and interpretation of XPS data* (pp. 84-85). Eden Prairie, MN: Physical Electronics. (1995)
- [29] Gandhi, V., Ganesan, R., Abdulrahman Syedahamed, H. H., & Thaiyan, M. Effect of cobalt doping on structural, optical, and magnetic properties of ZnO nanoparticles synthesized by coprecipitation method. *The Journal of Physical Chemistry C*, 118 (2014) 9715-9725.
- [30] Liu, W., Li, W., Hu, Z., Tang, Z., & Tang, X. Effect of oxygen defects on ferromagnetic of undoped ZnO. *Journal of Applied Physics*, 110 (2011) 013901.
- [31] Zandi, S., Kameli, P., Salamati, H., Ahmadvand, H., & Hakimi, M. Microstructure and optical properties of ZnO nanoparticles prepared by a simple method. *Physica B: Condensed Matter*, 406 (2011) 3215-3218.
- [32] Munoz-Hernández, G., Escobedo-Morales, A., & Pal, U. Thermolytic growth of ZnO nanocrystals: morphology control and optical properties. *Crystal Growth and Design*, 9 (2008) 297-300.
- [33]. Šimšíková, M., Antalík, M., Kaňuchová, M., & Škvarla, J. Cytochrome c conjugated to ZnO-MAA nanoparticles: The study of interaction and influence on protein structure. *International journal of biological macromolecules*, 59 (2013) 235-241.
- [34] Azam, A., Ahmed, A. S., Ansari, M. S., & Naqvi, A. H. Study of electrical properties of nickel doped SnO₂ ceramic nanoparticles. *Journal of Alloys and Compounds*, 506 (2010) 237-242.
- [35] J. Tauc, *Amorphous and Liquid Semiconductors*, ed., J. Tauc (Plenum, London, New York, 1974) p. 173.
- [36] H. Van cong, S. Charar, S. Brunet, *Phys. Status Sol. B*. 147 (2006) 253-258.

- [37] Yogamalar, N. R., & Bose, A. C. Absorption–emission study of hydrothermally grown Al: ZnO nanostructures. *Journal of Alloys and Compounds*, 509 (2011) 8493-8500.
- [38] Lu, J. G., Fujita, S., Kawaharamura, T., Nishinaka, H., Kamada, Y., Ohshima, T., ... & He, H. P. Carrier concentration dependence of band gap shift in n-type ZnO: Al films. *Journal of Applied Physics*, 101 (2007) 83705-83705.
- [39] P. Banerjee, W. J. Lee, K. R. Bae, S. B. Lee, G. W. Rubloff, *J. Appl. Phys.* 108 (2010) 0430705-43507.
- [40] Xu, P. S., Sun, Y. M., Shi, C. S., Xu, F. Q., & Pan, H. B. The electronic structure and spectral properties of ZnO and its defects. *Nuclear Instruments and Methods in Physics Research Section B: Beam Interactions with Materials and Atoms*, 199 (2003) 286-290.
- [41] Bylander, E. G. Surface effects on the low-energy cathodoluminescence of zinc oxide. *Journal of Applied Physics*, 49 (1978) 1188-1195.
- [42] Liu, M., Kitai, A. H., & Mascher, P. (1992). Point defects and luminescence centres in zinc oxide and zinc oxide doped with manganese. *Journal of Luminescence*, 54 (1992) 35-42.
- [43] Chen, Y. W., Liu, Y. C., Lu, S. X., Xu, C. S., Shao, C. L., Wang, C., ... & Fan, X. W. Optical properties of ZnO and ZnO: In nanorods assembled by sol-gel method. *The Journal of chemical physics*, 123 (2005) 134701.
- [44] Li, P., Wang, S., Li, J., & Wei, Y. Structural and optical properties of Co-doped ZnO nanocrystallites prepared by a one-step solution route. *Journal of Luminescence*, 132 (2012) 220-225.
- [45] Letailleur, A. A., Grachev, S. Y., Barthel, E., Søndergård, E., Nomenyo, K., Couteau, C., ... & Peter, E. High efficiency white luminescence of alumina doped ZnO. *Journal of Luminescence*, 131 (2011) 2646-2651.
- [46] Fan, X. M., Lian, J. S., Zhao, L., & Liu, Y. H. Single violet luminescence emitted from ZnO films obtained by oxidation of Zn film on quartz glass. *Applied surface science*, 252 (2005) 420-424.
- [47] Zhang, J., Sun, L., Yin, J., Su, H., Liao, C., & Yan, C. Control of ZnO morphology via a simple solution route. *Chemistry of Materials*, 14 (2002) 4172-4177.
- [48] Mishra, S. K., Srivastava, R. K., Prakash, S. G., Yadav, R. S., & Panday, A. C. Photoluminescence and photoconductive characteristics of hydrothermally synthesized ZnO nanoparticles. *Opto-Electronics Review*, 18 (2010) 467-473.
- [49] Jin, C. F., Yuan, X., Ge, W. W., Hong, J. M., & Xin, X. Q. Synthesis of ZnO nanorods by solid state reaction at room temperature. *Nanotechnology*, 14 (2003) 667.
- [50] Vanheusden, K., Seager, C. H., Warren, W. T., Tallant, D. R., & Voigt, J. A. Correlation between photoluminescence and oxygen vacancies in ZnO phosphors. *Applied Physics Letters*, 68 (1996)403-405.
- [51] Wu, D., Huang, Z., Yin, G., Yao, Y., Liao, X., Han, D., & Gu, J. Preparation, structure and properties of Mn-doped ZnO rod arrays. *CrystEngComm*, 12 (2010) 192-198.

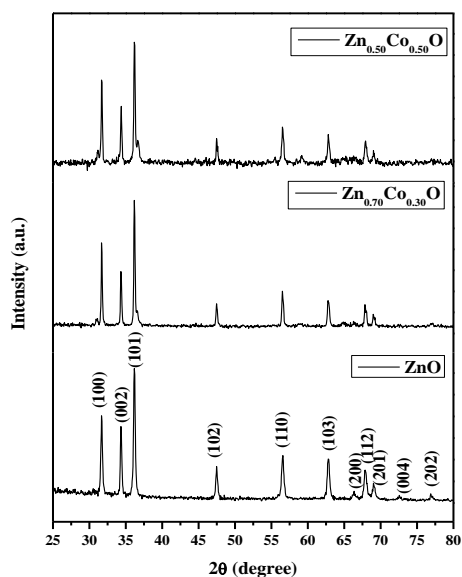


Figure 1 X-ray powder diffraction patterns of pure, Zn_{0.70}Co_{0.30}O and Zn_{0.50}Co_{0.50}O NPs.

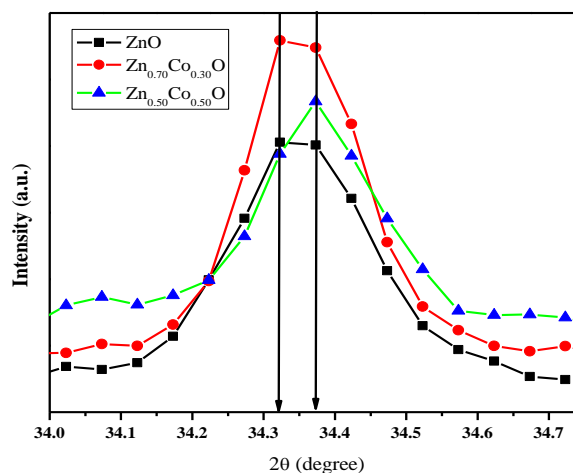


Figure. 1b X-ray powder diffraction pattern of an enlarged version of the XRD pattern between 35.8° and 37°

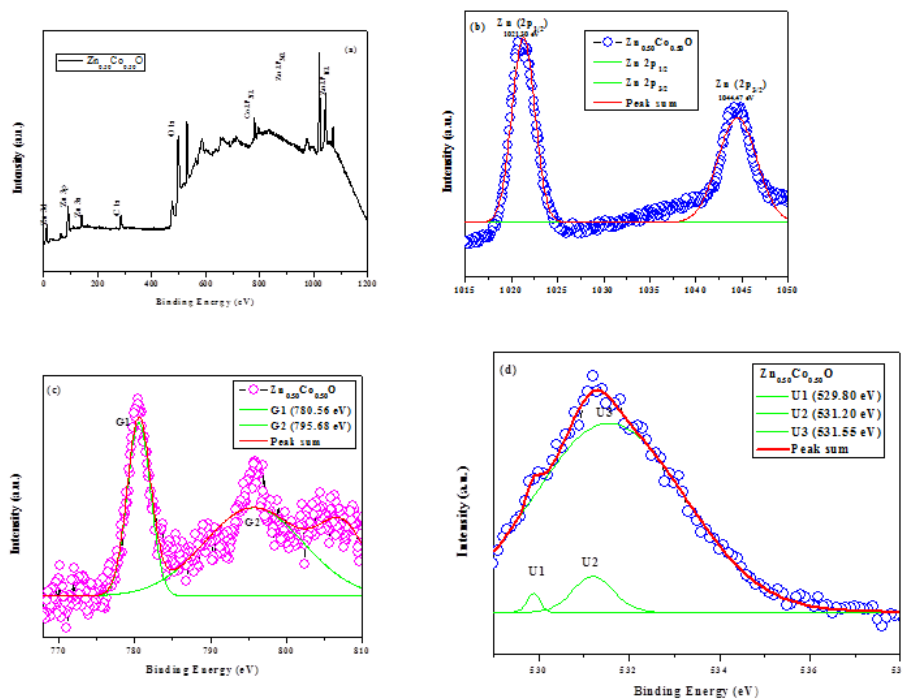


Figure 2 XPS spectra of (a) Zn_{0.50}Co_{0.50}O wide survey, (b) Zn 2p, (c) Co 2p, and (d) O 1s of Co-doped ZnO NPs.

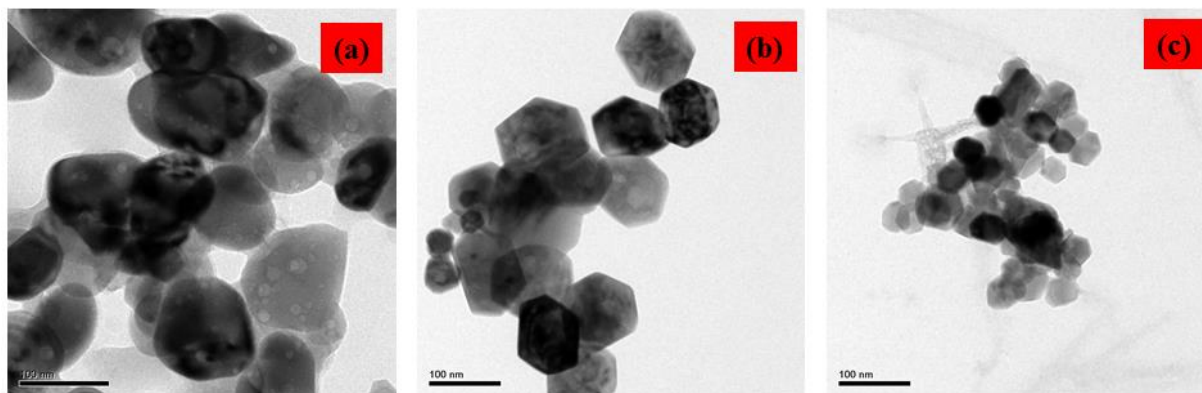


Figure 3 (a-c) TEM images of (a) pure (b) Zn_{0.70}Co_{0.30}O, and (c) Zn_{0.50}Co_{0.50}O NPs

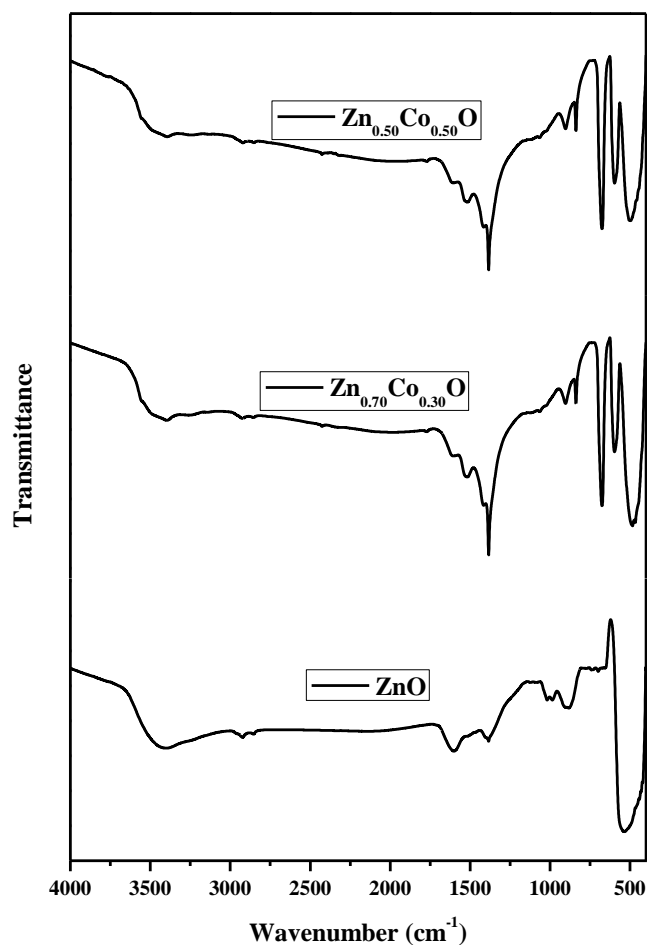


Figure 4 FT-IR absorption spectra of pure, Zn_{0.70}Co_{0.30}O and Zn_{0.50}Co_{0.50}O NPs

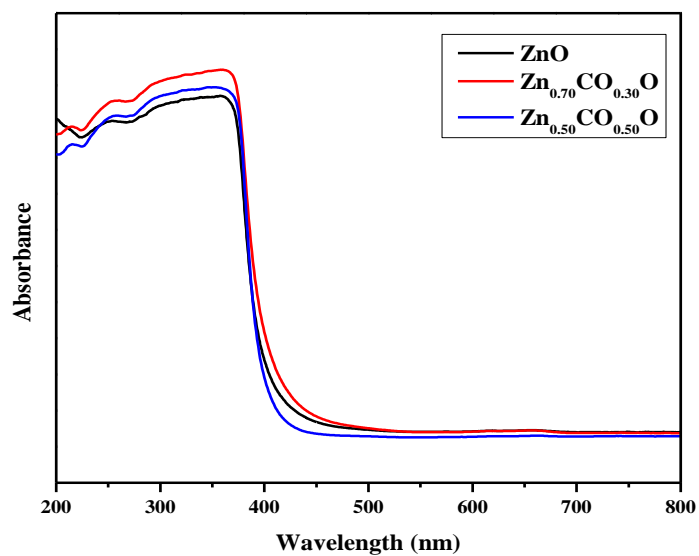


Figure 5 UV-vis spectra of pure, Zn_{0.70}Co_{0.30}O and Zn_{0.50}Co_{0.50}O NPs

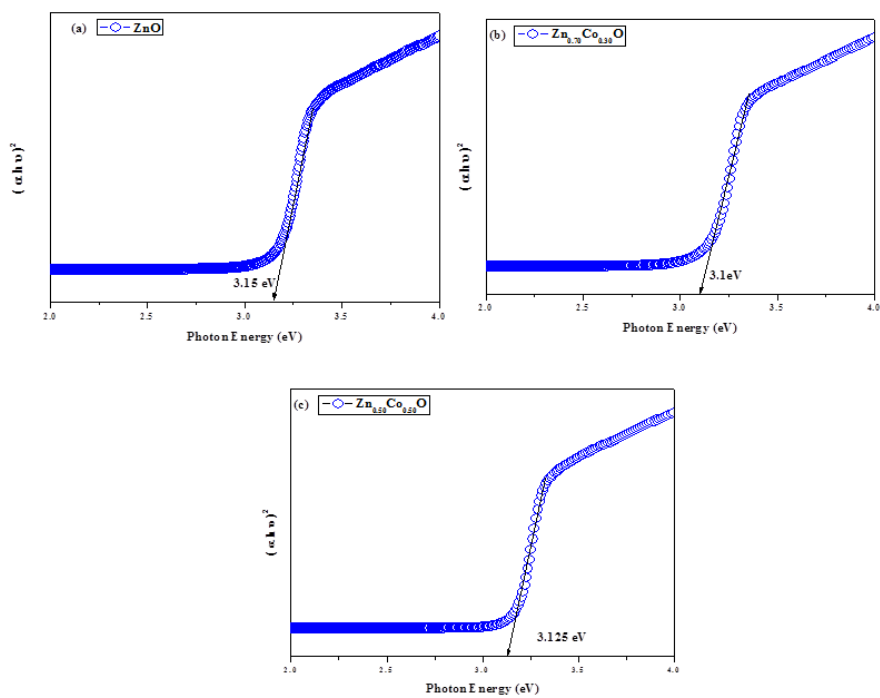


Figure 5 Band gap measurement for n = 1 excitonic state of (a) pure, (b) Zn_{0.70}Co_{0.30}O and (c) Zn_{0.50}Co_{0.50}O NPs

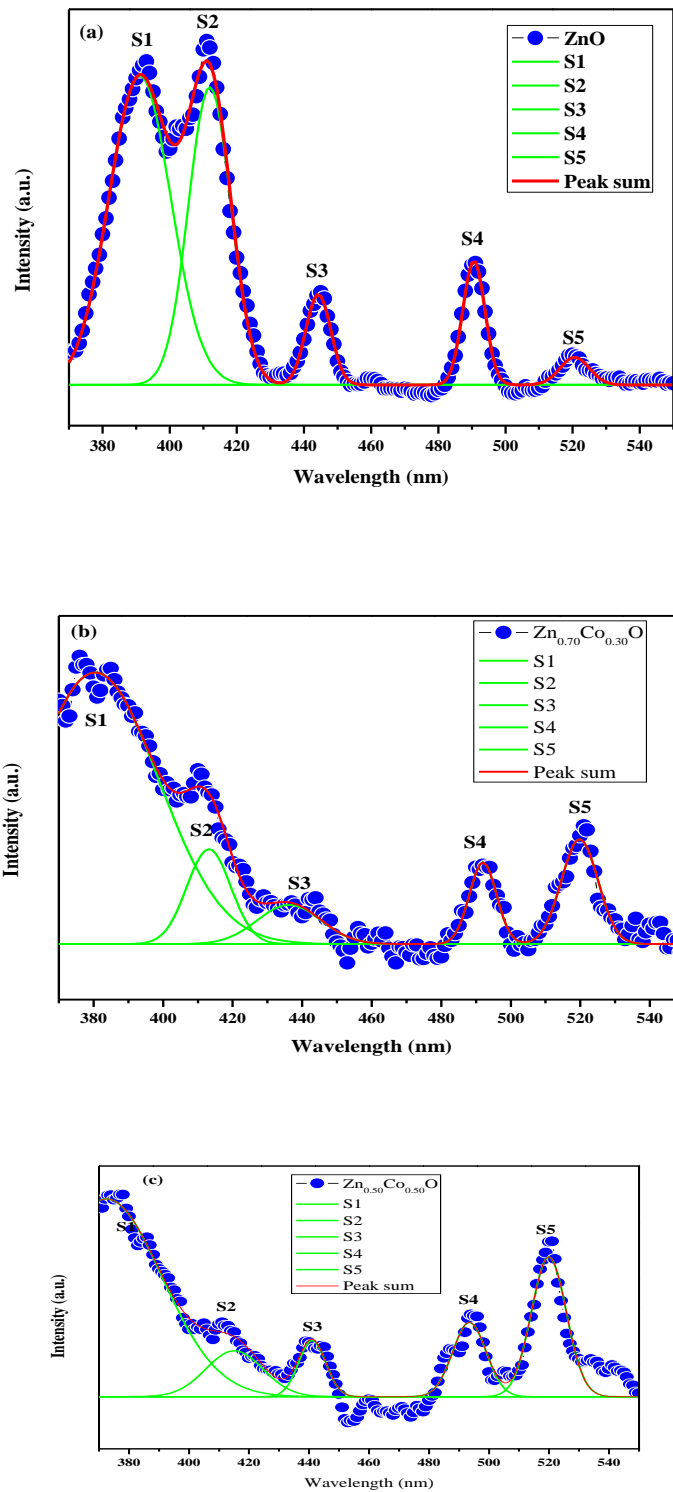


Figure 6 Gaussian de-composed photoluminescence emission spectra of (a) Pure ZnO (b) Zn_{0.70}Co_{0.30}O and (c) Zn_{0.50}Co_{0.50}O NPs

JCPDS Card no: (79-2205) 2θ (degree)	ZnO 2θ (degree)	Zn _{0.70} Co _{0.30} O 2θ (degree)	Zn _{0.50} Co _{0.50} O 2θ (degree)	JCPDS Card no: (79-2205) d-spacing [Å]	ZnO d-spacing [Å]	Zn _{0.70} Co _{0.30} O d-spacing [Å]	Zn _{0.50} Co _{0.50} O d-spacing [Å]
31.799	31.6864	31.7038	31.7115	2.8146	2.82389	2.82237	2.82171
34.419	34.3505	34.3568	34.3822	2.6035	2.61073	2.61027	2.60840
36.251	36.1772	36.1826	36.1998	2.4760	2.48299	2.48263	2.48149
-	-	-	36.6973	-	-	-	2.44899
47.536	47.4600	47.4901	47.4793	1.9112	1.91572	1.91457	1.91499
56.591	56.5424	56.5129	56.5246	1.6250	1.62767	1.62845	1.62814
-	-	58.9222	59.2929	-	-	1.56748	1.55856
62.851	62.8202	62.7745	62.8188	1.4773	1.47927	1.48024	1.47930
66.371	66.3253	66.3700	-	1.4073	1.40935	1.40850	-
67.942	67.9043	67.8377	67.8904	1.3785	1.38037	1.38156	1.38062
69.081	69.0635	69.0055	69.0691	1.3585	1.36001	1.36101	1.35991
76.953	76.9893	76.9064	-	1.2380	1.23857	1.23970	-

Table 1a As compared ZnO NPs and JCPDS data values.

FWHM β (°)			(hkl)	JCPDS Card no: (79- 2205) Relative Intensity	ZnO Relative Intensity	Zn _{0.70} Co _{0.30} O Relative Intensity	Zn _{0.50} Co _{0.50} O Relative Intensity
ZnO	Zn _{0.70} Co _{0.30} O	Zn _{0.50} Co _{0.50} O					
0.1968	0.1476	0.1476	(100)	56.40	61.82	62.06	67.74
0.1968	0.1476	0.1968	(002)	41.50	54.89	43.31	45.89
0.2460	0.1968	0.1476	(101)	99.99	100.00	100.00	100.00
	-	0.1968			-	-	17.35
0.1968	0.1968	0.1476	(102)	21.10	24.62	17.29	20.21
0.2460	0.2460	0.2460	(110)	30.50	32.91	28.24	29.96
	1.1808	0.5904				1.81	4.68
0.2952	0.2952	0.2952	(103)	26.80	31.59	20.80	23.82
0.3936	0.5904	-	(200)	4.00	4.96	2.75	-
0.3444	0.1968	0.2460	(112)	21.70	22.23	18.17	18.17
0.2460	0.1476	0.2460	(201)	10.6	11.59	9.58	8.06
0.3936	0.5904	-	(202)	3.30	2.84	1.97	-

Table 1b As compared ZnO NPs and JCPDS data values.

Sample	Lattice Parameter values (Å)		Atomic Packing factor (c/a)	Average Crystallite size D (nm)
	a	C		
ZnO	3.2607	5.2214	1.6013	33
Zn _{0.70} Co _{0.30} O	3.2589	5.2205	1.6019	42
Zn _{0.50} Co _{0.50} O	3.2582	5.2168	1.6011	41

Table 2 The XRD parameter values of pure, Zn_{0.70}Co_{0.30}O and Zn_{0.50}Co_{0.50}O NPs.

ZnO (nm)	Zn _{0.70} Co _{0.30} O (nm)	Zn _{0.50} Co _{0.50} O (nm)	Assignment
3398	3397	3393	O-H stretching
2923	2923	-	C-H asymmetric stretching
-	1518	1518	C=O asymmetric stretching
-	1415	1415	C=O symmetric stretching
884	838	838	Weak vibration of ZnO
699	675	675	Zn-O bending
533	597	597	Zn-O stretching
442, 421	485, 466	495	Zn-O stretching

Table 3. FTIR Peak Assignments of pure, Zn_{0.70}Co_{0.30}O and Zn_{0.50}Co_{0.50}O NPs

Sample code	ZnO (nm)	Zn _{0.70} Co _{0.30} O (nm)	Zn _{0.50} Co _{0.50} O (nm)	Assignment
S1	391	380	372	Near Band Edge emission
S 2	411	413	415	Violet emission
S 3	444	436	441	Blue emission
S 4	490	492	493	Blue-green emission
S 5	519	520	520	Green emission

Table 4 Comparison of the PL emission values of the pure, Zn_{0.70}Co_{0.30}O and Zn_{0.50}Co_{0.50}O NPs.